Int J Adv Manuf Technol (2016) 87:3497–3512
DOI 10.1007/s00170-016-8692-3

ORIGINAL ARTICLE

Investigation of porous coatings obtained on Ti-Nb-Zr-Sn alloy biomaterial by plasma electrolytic oxidation: characterisation and modelling

Krzysztof Rokosz[1] · **Tadeusz Hryniewicz**[1] · **Steinar Raaen**[2] · **Patrick Chapon**[3]

Received: 23 December 2015 / Accepted: 27 March 2016 / Published online: 15 April 2016

Abstract In the paper, the fabrication method and characteristics of porous coatings on Ti-Nb-Zr-Sn alloy biomaterial obtained by plasma electrolytic oxidation (PEO) are presented. The PEO process was performed at two voltages of 180 ± 10 and 450 ± 10 V, respectively, during 3 min of treatment in the electrolyte based on orthophosphoric acid with copper II nitrate of initial temperature of 20 ± 2 °C. Scanning electron microscopy (SEM) with energy-dispersive X-ray spectroscopy (EDS), glow discharge optical emission spectroscopy (GDOES), X-ray photoelectron spectroscopy (XPS) and 2D roughness measurements were performed on the samples. The study results indicate an enrichment of the porous layer (18 and 21 μm thick, for 180 and 450 V, respectively) in two elements, P and Cu, coming from the electrolyte used. The analysis performed based on the SEM, EDS, GDOES and XPS results obtained shows that after the PEO treatment, three sub-layers of the coating can be distinguished and separated and two models are proposed to fit these findings. It was found that both the contents of copper and phosphorus in the surface layer as well as the thickness of porous coating can be controlled to some extent by the PEO parameters. The greatest achievement of the presented work is the lack of toxic tin inside the top surface layer of the porous coatings as well as the enrichment of the coatings with copper ions up to 2.3 at%. In authors' opinion, the finding of the transition layer enriched within hydrogen and nitrogen ions can be interpreted by the presence of molecules of phosphoric acid and copper nitrate occurring in that sub-layer. This is a great advancement in the field of identification of the layers obtained by PEO.

Keywords Plasma electrolytic oxidation (PEO)/micro arc oxidation (MAO) · Titanium-niobium-zirconium-tin alloy · SEM · XPS · GDOES · Porous coating · Copper enrichment

✉ Tadeusz Hryniewicz
Tadeusz.Hryniewicz@tu.koszalin.pl

Krzysztof Rokosz
rokosz@tu.koszalin.pl

Steinar Raaen
steinar.raaen@ntnu.no

Patrick Chapon
patrick.chapon@horiba.com

[1] Division of Surface Electrochemistry & Technology, Faculty of Mechanical Engineering, Koszalin University of Technology, Racławicka 15-17, PL 75-620 Koszalin, Poland

[2] Department of Physics, Norwegian University of Science and Technology (NTNU), Realfagbygget E3-124 Høgskoleringen 5, NO 7491 Trondheim, Norway

[3] HORIBA Jobin Yvon S.A.S., 16-18, rue du Canal, 91165 Longjumeau cedex, France

1 Introduction

Plasma electrolytic oxidation (PEO), known also as micro arc oxidation (MAO) or spark anodisation (SA) [1–10], is very often used for formation of micro-coatings (about 10 μm thick) on metals (titanium, niobium, zirconium, tantalum) [1–5] and their alloys [5–10], with nano- and micro-pores. Other much thinner nano-layers (about 5–10 nm) can be obtained by electropolishing (EP) [11–15], magnetoelectropolishing (MEP) [16–23] and a high-current density

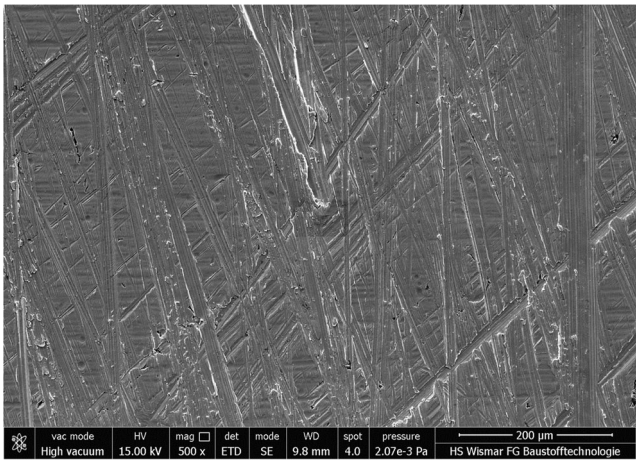

Fig. 1 SEM picture of sample surface formed on Ti-Nb-Zr-Sn alloy after mechanical pretreatment by means of SiC abrasive paper 120 grit size. Magnification 500 times

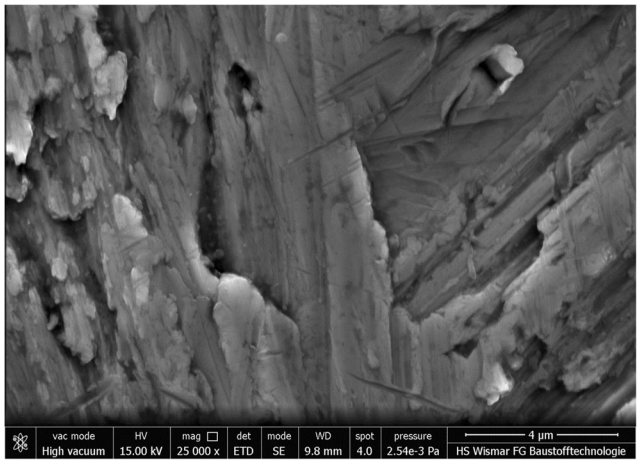

Fig. 3 SEM picture of sample surface formed on Ti-Nb-Zr-Sn alloy after mechanical pretreatment by means of SiC abrasive paper 120 grit size. Magnification 25,000 times

electropolishing (HDEP) [24, 25], which may be used for surface preparation of biomaterials for PEO oxidation. All mentioned electrochemical treatments are widely used in the biomedical industry, to make the metallic materials surface more biocompatible [26], inter alia because of their better corrosion resistance [27] and compatible with human tissue chemical compositions [28–32].

The results in the present paper are a continuation of our work presented in [10], in which porous and biocompatible coatings obtained on Ti6Al4V alloy biomaterial, enriched in bactericidal copper [33–38] and depleted in vanadium and aluminium ions, were described. In this article, the authors present the PEO coatings obtained on another very popular alloy, i.e. titanium-niobium-zirconium-tin, which is often advised for use as biomaterial. The elements titanium, niobium and zirconium are totally biocompatible, but tin can be toxic for human tissue [39].

The data displayed in this paper were obtained by different research methods, such as scanning electron microscopy (SEM) and energy-dispersive X-ray spectroscopy (EDS) complemented by glow discharge optical electron spectroscopy (GDOES) and X-ray photoelectron spectroscopy (XPS). Besides, two-dimensional profiles of the coatings formed on the Ti-Nb-Zr-Sn alloy after 3-min PEO treatment at voltages of 180 and 450 V are also presented.

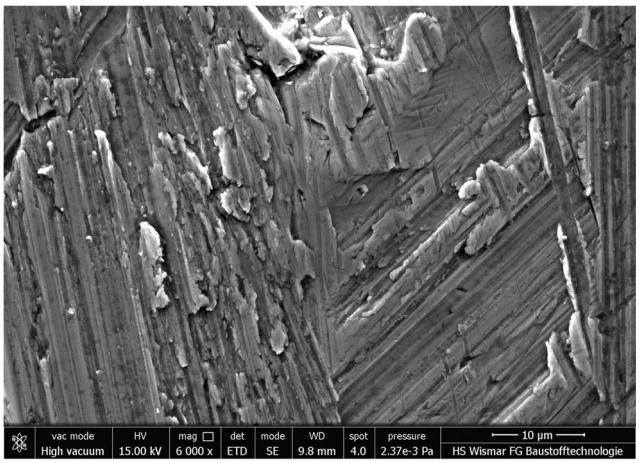

Fig. 2 SEM picture of sample surface formed on Ti-Nb-Zr-Sn alloy after mechanical pretreatment by means of SiC abrasive paper 120 grit size. Magnification 6000 times

2 Method

2.1 Material

Titanium-niobium-zirconium-tin alloy samples mechanically polished with SiC abrasive paper of 120 grit size were used as input material for the PEO treatment. The samples were prepared in the form of rectangular specimens of dimensions 10 × 35-mm cut-off from an alloy sheet 1 mm thick. In Figs. 1, 2 and 3, the SEM images of samples after mechanical polishing with different magnifications, i.e. ×500, ×6000 and ×25,000, are presented. In the pictures, the characteristic marks of abrasive treatment are visible. In Fig. 4, the EDS spectrum of the mechanically treated surface and the chemical

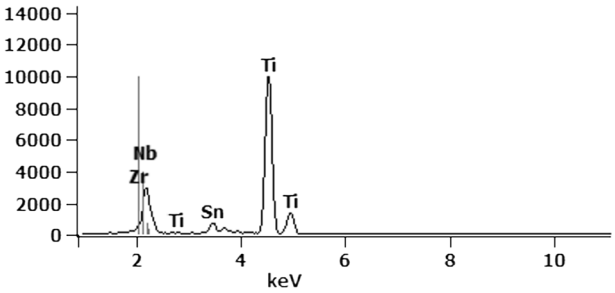

Element	at%
Ti K	88.4
Zr K	1.0
Nb K	6.7
Sn L	3.9

Fig. 4 EDS results of Ti-Nb-Zr-Sn alloy surface after abrasive pretreatment

composition are shown. On the basis of the obtained EDS results, it can be concluded that the measured chemical composition differs from the assumed (Ti-24Nb-4Zr-8Sn) alloy. The measured alloy composition has a lower amount of niobium (11.6 wt%|6.7 at%), zirconium (1.7 wt%|1 at%) and a slightly higher amount of tin (8.6 wt%|3.9 at%).

2.2 Set-up and parameters

The PEO was performed at voltages of 180 ± 10 and 450 ± 10 V, respectively, during 3 min of treatment. For the studies, we decided to take two voltages which allow to obtain stable plasma at lower voltage (180 V) and at maximum available voltage, i.e. 450 V. Time of the treatment was taken as 3 min, because of the previously evaluated coating porosity [40, 41]. Based on the earlier exploratory research on titanium, authors decided that the PEO treatment for 3 min affords obtaining a repeatable porous coating.

The studies were carried out in the electrolyte of initial temperature of 20 ± 2 °C. For the studies, an electrolyte composed of concentrated (85 %) orthophosphoric acid (1 L), with an addition of and 600 g of copper II nitrate, was used. For each run, an electrolytic cell made of glass was used, containing up to 500 mL of the electrolyte.

2.3 SEM and EDS studies

The scanning electron microscope Quanta 250 FEI with low vacuum and ESEM mode and a field emission cathode, as well as the energy-dispersive EDX system in a Noran System Six with nitrogen-free silicon drift detector, was employed. The magnifications of 500 and 6000 times for SEM surface images were used. The EDS analyses were performed from the whole frame at magnification of 6000 times. The separation of phosphorus (P_K 2.013 eV) and zirconium (Zr_L 2.042 eV), especially with very close niobium signal (Nb_L 2.166 eV) in EDS measurement, is not possible without significant errors. Obviously, the software may separate the phosphorus and zirconium signals based on algorithms, but in the authors' opinion, it is not the ideal solution and

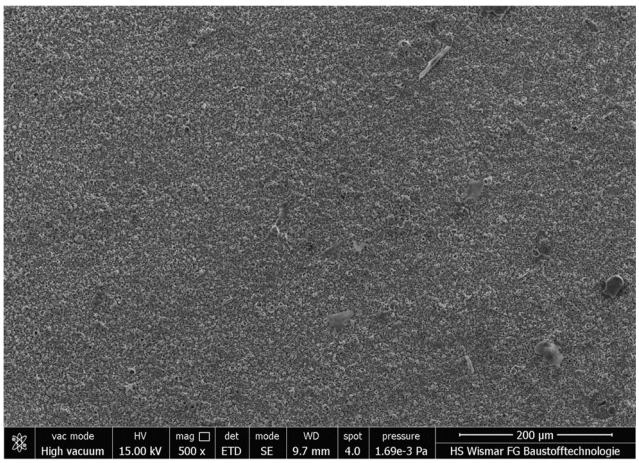

Fig. 5 SEM picture of coating formed on Ti-Nb-Zr-Sn alloy surface after PEO treatment at voltage of 180 V in 3.2 mol/L of $Cu(NO_3)_2$ in H_3PO_4 electrolyte. Magnification 500 times

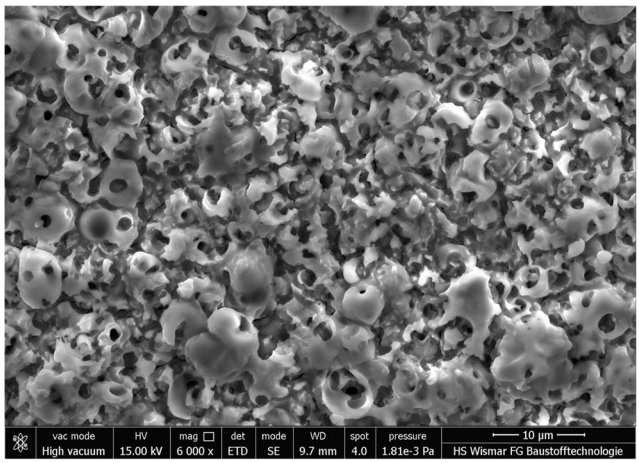

Fig. 6 SEM picture of coating formed on Ti-Nb-Zr-Sn alloy surface after PEO treatment at voltage of 180 V in 3.2 mol/L of $Cu(NO_3)_2$ in H_3PO_4 electrolyte. Magnification 6000 times

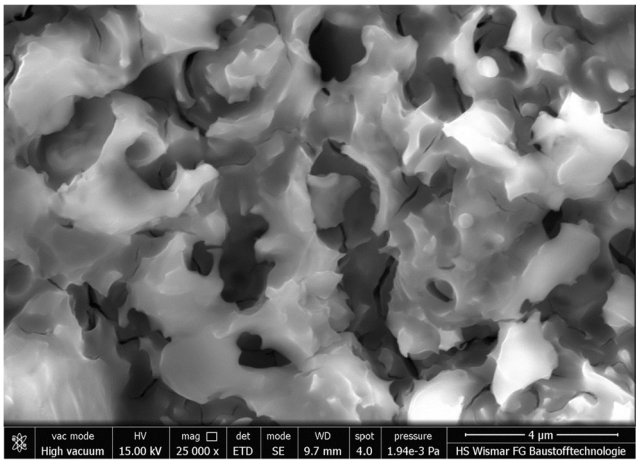

Fig. 7 SEM picture of coating formed on Ti-Nb-Zr-Sn alloy surface after PEO treatment at voltage of 180 V in 3.2 mol/L of $Cu(NO_3)_2$ in H_3PO_4 electrolyte. Magnification 25,000 times

could cause errors in the interpretation of the results. This is why at this stage of the study, chemical elements, such as phosphorus and zirconium, will be presented as an atomic percentage value.

2.4 XPS studies

The X-ray photoelectron spectroscopy (XPS) measurements on Ti-Nb-Zr-Sn alloy samples' surfaces were performed by means of SCIENCE SES 2002 instrument using a monochromatic (Gammadata-Scienta) Al K(alpha) ($h\nu = 1486.6$ eV) X-ray source (18.7 mA, 13.02 kV). Scan analyses were carried out with an analysis area of 1×3 mm and a pass energy of 500 eV with the energy step 0.2 eV and step time 200 ms. The binding energy of the spectrometer has been calibrated by the position of the Fermi level on a clean metallic sample. The power supplies were stable and of high accuracy. The experiments were carried out in an ultra-high-vacuum system with a base pressure of about $6 \cdot 10^{-8}$ Pa. The XPS spectra were recorded in normal emission. For the XPS analyses, the CasaXPS 2.3.14 software (Shirley background type) [42], with the help of XPS tables [43–46], was used. All the binding energy values presented in this paper were charge corrected to C 1s at 284.8 eV.

2.5 GDOES studies

The glow discharge optical emission spectroscopy (GDOES) measurements on PEO-oxidized Ti-Nb-Zr-Sn alloy samples were performed by Horiba Scientific Profiler 2 instrument using RF asynchronous pulse generator under the plasma conditions (pressure 700 Pa, power 40 W, frequency 3000 Hz, duty cycle 0.25, anode diameter 4 mm). The signals of copper (325 nm), phosphorus (178 nm), oxygen (130 nm), nitrogen (149 nm), hydrogen (122 nm), titanium (365 nm), niobium (316 nm), zirconium (360 nm) and tin (190 nm) were measured.

2.6 2D roughness measurements

A computerized HOMMEL TESTER T800 system of Hommelwerke GmbH study of surface roughness measurement and GDOES crater depth was used. It was equipped with sliding measuring head Waveline 60 Basic/51808 and the sensor TKL100/17 MO435005. Measuring needle beam was equal to 3.5 µm with its angle of 87°. The tracing, evaluation and single measuring lengths equal to 4.8, 4.0 and 0.8 mm, respectively. Due to the porous surface, the non-contact methods for surface roughness [47] were not possible to be used, inter alia because of the uncertainties in measurement results [48]. According to the EN ISO 4287:1999 [49] and DIN 4768 [50] standards, the following roughness parameters have been measured: arithmetic mean of the sum of roughness profile values (Ra), mean peak-to-valley height (Rz^{DIN}), ten-point height (Rz^{ISO}), root-

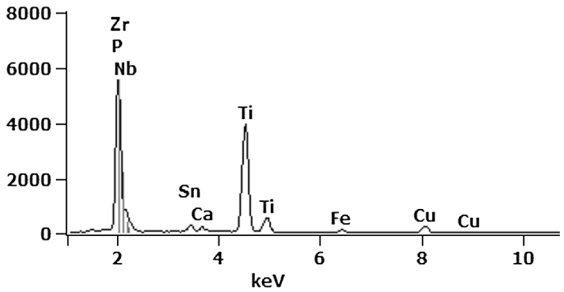

180 V	
Element	*at%*
O K	71.2
P K & Zr L	14.8
Ti K	11.5
Cu K	1.3
Nb K	0.7
Sn L	0.5

Fig. 8 EDS results of coating formed on Ti-Nb-Zr-Sn alloy surface after PEO treatment at voltage of 180 V in 3.2 mol/L of $Cu(NO_3)_2$ in H_3PO_4 electrolyte

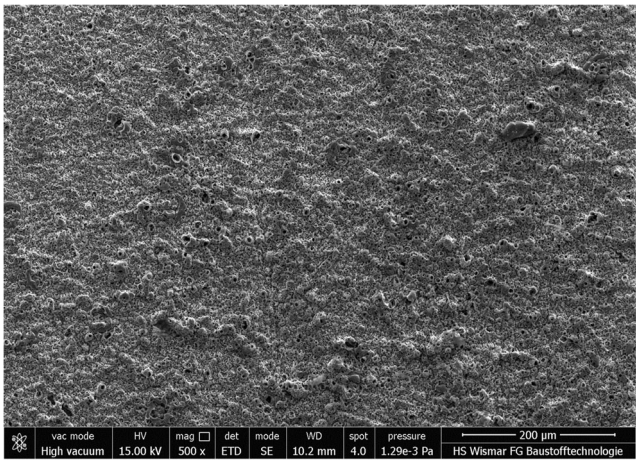

Fig. 9 SEM picture of coating formed on Ti-Nb-Zr-Sn alloy surface after PEO treatment at voltage of 450 V in 3.2 mol/L of $Cu(NO_3)_2$ in H_3PO_4 electrolyte. Magnification 500 times

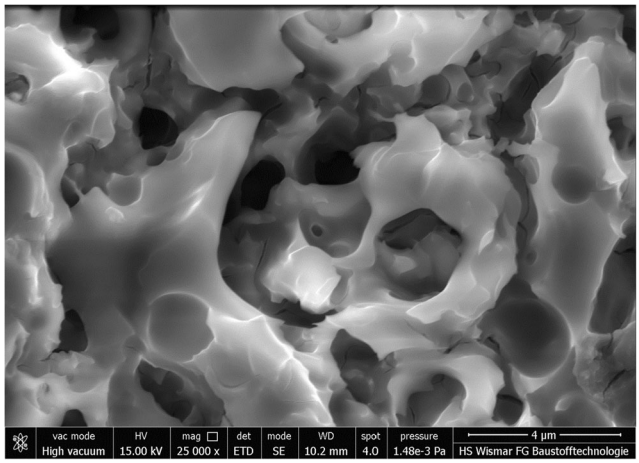

Fig. 11 SEM picture of coating formed on Ti-Nb-Zr-Sn alloy surface after PEO treatment at voltage of 450 V in 3.2 mol/L of $Cu(NO_3)_2$ in H_3PO_4 electrolyte. Magnification 25,000 times

mean-square deviation of the roughness profile (Rq), total height of the roughness profile (Rt), mean width of the roughness profile elements (RSm), the ratio of the developed profile length to the evaluation length (L_0) and profile peak density (D).

3 Results and discussion

In Figs. 5, 6 and 7, the SEM pictures of coating formed on Ti-Nb-Zr-Sn alloy surface after PEO treatment at voltage of 180 V in 3.2 mol/L of $Cu(NO_3)_2$ in H_3PO_4 electrolyte with different magnifications, i.e. ×500, ×6000 and ×25,000, are presented. The obtained surface is porous and composed mainly of phosphorus and zirconium (14.8 at%), titanium (11.5 at%) and oxygen (71.2 at%) within lower amounts of copper (1.3 at%), niobium (0.7 at%) and tin (0.5 at%), as displayed in Fig. 8. The pores are mostly opened with noticeable cracks in the PEO coating surface that are best visible under the highest magnification, i.e. ×25,000 (Fig. 7).

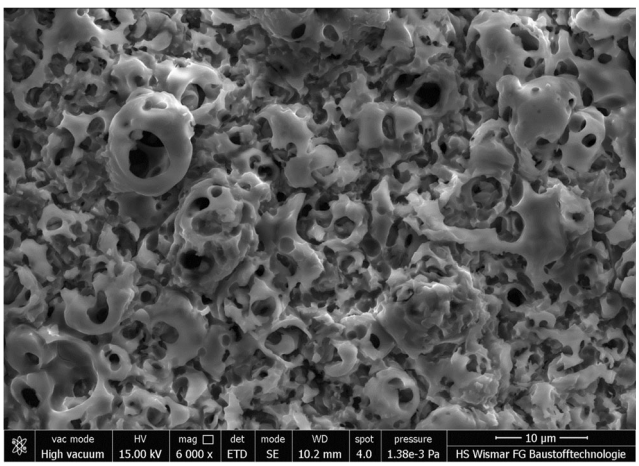

Fig. 10 SEM picture of coating formed on Ti-Nb-Zr-Sn alloy surface after PEO treatment at voltage of 450 V in 3.2 mol/L of $Cu(NO_3)_2$ in H_3PO_4 electrolyte. Magnification 6000 times

In Figs. 9, 10 and 11, the SEM images of coating formed on Ti-Nb-Zr-Sn alloy surface after PEO treatment at voltage of 450 V in 3.2 mol/L of $Cu(NO_3)_2$ in H_3PO_4 electrolyte with different magnifications, i.e. ×500, ×6000 and ×25,000, are given. The obtained surface is porous and composed mainly of phosphorus and zirconium (13.1 at%), titanium (9.5 at%) and oxygen (75.4 at%) within lower amounts of copper (1.1 at%), niobium (0.6 at%) and tin (0.3 at%), as presented in Fig. 12. In Fig. 11, with the magnification equalling ×25,000, some smaller pores inside the bigger ones are visible.

The data presented in Figs. 8 and 12 display the differences between the coatings formed during PEO process on Ti-Nb-Zr-Sn alloy surface in concentrated phosphoric acid within copper nitrate using the two different voltages, i.e. 180 and 450 V, respectively. One may easily notice that after PEO treatment at 450 V, the PEO coating contains a higher amount of oxygen, but lower amounts of titanium, copper, niobium, phosphorus|zirconium and tin. In case of the coating obtained after the PEO treatment at 180 V, higher amounts of titanium, copper and tin were recorded

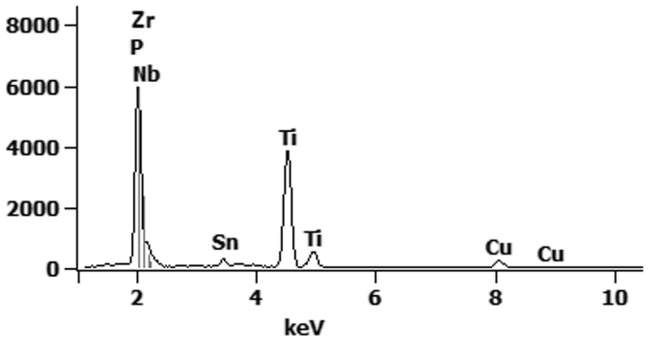

450 V	
Element	*at%*
O K	75.4
P K & Zr L	13.1
Ti K	9.5
Cu K	1.1
Nb K	0.6
Sn L	0.3

Fig. 12 SEM picture of coating formed on Ti-Nb-Zr-Sn alloy surface after PEO treatment at voltage of 450 V in 3.2 mol/L of $Cu(NO_3)_2$ in H_3PO_4 electrolyte

inside it. Concerning the biocompatibility aspects, all the obtained surfaces' chemical compositions are correct, and what is most important, the two obtained surfaces are porous. At this step of the study, the question of the uniform distribution of copper in the whole coating volume should be answered to determine at which PEO voltage a thicker coating is created. To answer these questions, the GDOES study was carried out, with the results presented in consecutive Figs. 13, 14, 15, 16, 17, 18, 19, 20 and 21.

In Fig. 13, two copper signals (325 nm) coming from PEO coatings obtained during the oxidation at 180 and 450 V are presented. It should be noted that after the PEO treatment at 450 V, the copper amount in the whole PEO coating volume is higher than that obtained after oxidation at 180 V. It is also noted that the PEO coating thickness obtained at 450 V is thicker than the one formed at 180 V. On the other hand, however, the PEO oxidation at 180 V features a local copper maximum, which is not so well visible on the sample treated at 450 V. In Figs. 14, 15 and 16, the GDOES spectra of phosphorus (178 nm), oxygen (130 nm) and nitrogen (149 nm) and hydrogen (122 nm), respectively, are shown. The amount of these chemical elements for both PEO treatments is quite similar. However, as it was already observed in all spectra of samples obtained under higher voltage, i.e. 450 V, the formation of a thicker PEO coating compared to the one created at 180 V was noted. Additionally, in copper, phosphorus, nitrogen and hydrogen profiles, there are clear visible maxima. Such results may suggest that the PEO coating contains a minimum of three sub-layers, i.e. outer (porous), medium (semi-porous) and transition (between coating and matrix). The analyses of titanium (365 nm), niobium (316 nm), zirconium (360 nm) and tin (190 nm) signals (Figs. 18, 19, 20 and 21) confirm the above-stated reasoning regarding the thicker coating obtained at a higher voltage (450 V) and the existence of the transition layer in there. It should be noted that the outer and porous sub-layer is enriched mainly with phosphorus, oxygen, nitrogen and hydrogen, which can suggest that a part of coating is also organically contaminated. The next semi-

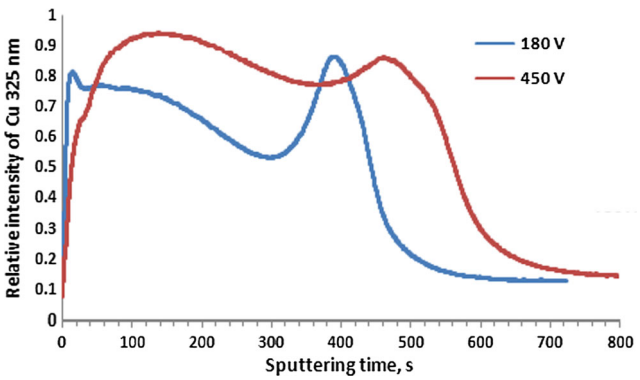

Fig. 13 GDOES results of copper signal (325 nm) of coating formed on Ti-Nb-Zr-Sn alloy after 3 min of PEO treatment at voltages of 180 and 450 V in electrolyte containing of H_3PO_4 within $Cu(NO_3)_2$

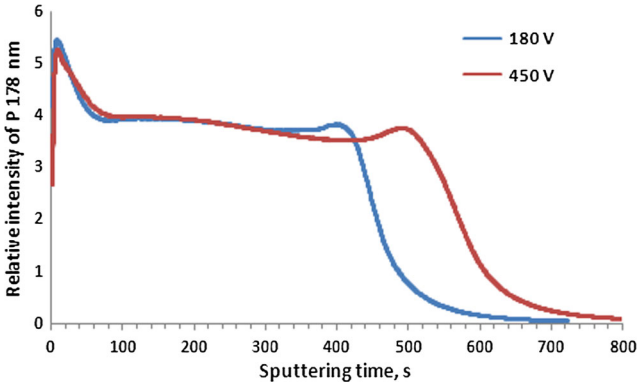

Fig. 14 GDOES results of phosphorus signal (178 nm) of coating formed on Ti-Nb-Zr-Sn alloy after 3 min of PEO treatment at voltages of 180 and 450 V in electrolyte containing of H_3PO_4 within $Cu(NO_3)_2$

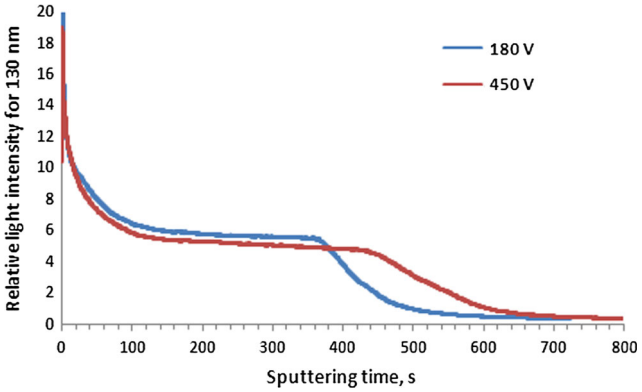

Fig. 15 GDOES results of oxygen signal (130 nm) of coating formed on Ti-Nb-Zr-Sn alloy after 3 min of PEO treatment at voltages of 180 and 450 V in electrolyte containing of H_3PO_4 within $Cu(NO_3)_2$

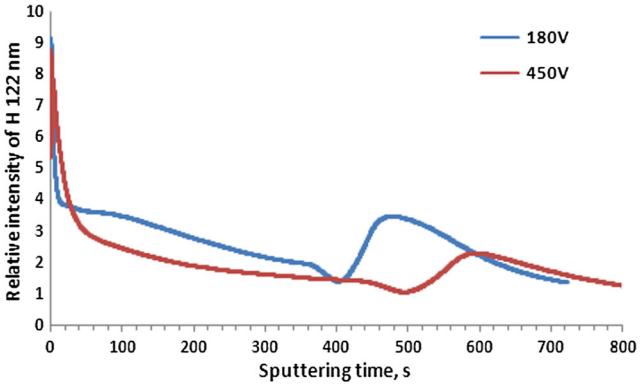

Fig. 17 GDOES results of hydrogen signal (122 nm) of coating formed on Ti-Nb-Zr-Sn alloy after 3 min of PEO treatment at voltages of 180 and 450 V in electrolyte containing of H_3PO_4 within $Cu(NO_3)_2$

porous sub-layer is the thickest one and composed mainly of phosphorus and oxygen as well as copper, nitrogen and hydrogen. The third sub-layer from the top surface, i.e. transition layer, is the most interesting, because it shows a different chemical composition. The copper, phosphorus, nitrogen and hydrogen maxima may suggest that in the structure of this sub-layer, there are molecules of both phosphoric acid and copper nitrate present.

In Fig. 22, an example of GD resulting-crater made on a coating formed on Ti-Nb-Zr-Sn alloy surface after 3 min of PEO treatment at voltage of 450 V in electrolyte containing of H_3PO_4 within $Cu(NO_3)_2$ is shown and used to estimate the correlation between the sputtering time during the GDOES process and the depth, assuming that the erosion rate does not change much in the coating. On the basis of the obtained data, it can be said that a sputtering time of 100 s corresponds to a thickness of about 3 μm. Therefore, it follows that the PEO coating obtained at 180 V is composed of 3-μm outer porous sub-layer, 9-μm semi-porous layer and 6-μm transition layer. In case of coating formed at 450 V, the thickness of outer porous sub-layer is also about 3 μm, the semi-porous sub-layer thickness equals 12 μm, and the transition sub-layer is about 6 μm thick.

In Fig. 23, it is shown the example of two-dimensional profiles of the coatings formed on Ti-Nb-Zr-Sn alloy after 3-min PEO treatment at voltages of 180 and 450 V in electrolyte composed of H_3PO_4 within $Cu(NO_3)_2$. In Tables 1 and 2 as well as in Fig. 24, the roughness parameters of PEO coating formed on Ti-Nb-Zr-Sn alloy at 180 and 450 V, respectively, are presented. Based on these results, it should be concluded that the surface roughness after PEO treatment at 180 V is lower than that after the oxidation at 450 V. It can provide also some information about the porosity of the

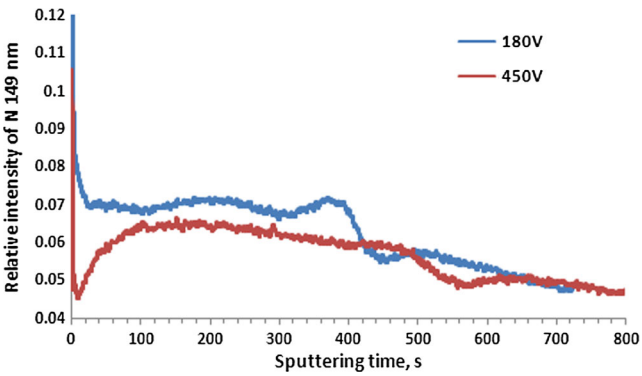

Fig. 16 GDOES results of nitrogen signal (149 nm) of coating formed on Ti-Nb-Zr-Sn alloy after 3 min of PEO treatment at voltages of 180 and 450 V in electrolyte containing of H_3PO_4 within $Cu(NO_3)_2$

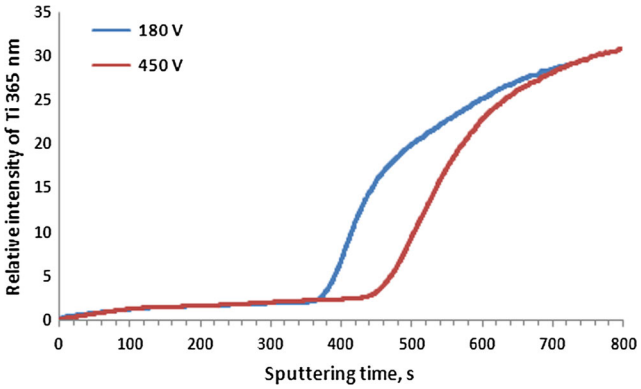

Fig. 18 GDOES results of titanium signal (365 nm) of coating formed on Ti-Nb-Zr-Sn alloy after 3 min of PEO treatment at voltages of 180 and 450 V in electrolyte containing of H_3PO_4 within $Cu(NO_3)_2$

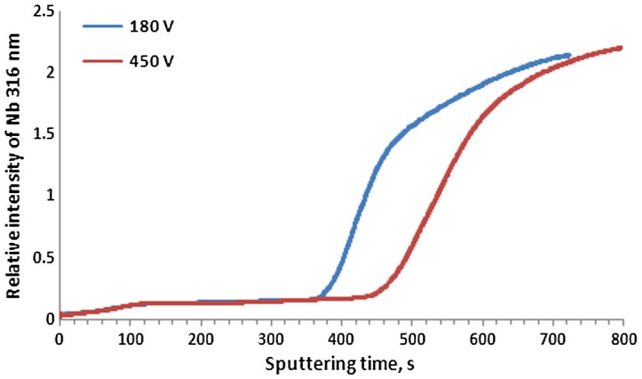

Fig. 19 GDOES results of niobium signal (316 nm) of coating formed on Ti-Nb-Zr-Sn alloy after 3 min of PEO treatment at voltages of 180 and 450 V in electrolyte containing of H_3PO_4 within $Cu(NO_3)_2$

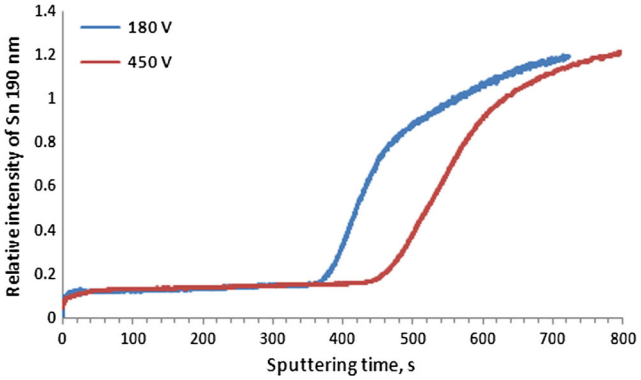

Fig. 21 GDOES results of tin signal (190 nm) of coating formed on Ti-Nb-Zr-Sn alloy after 3 min of PEO treatment at voltages of 180 and 450 V in electrolyte containing of H_3PO_4 within $Cu(NO_3)_2$

obtained PEO coatings; i.e. the higher the roughness parameter is, the bigger pores are observed, what is confirmed by SEM and roughness studies. In case of significance tests, the null hypothesis H_0 must be formulated; i.e. it is assumed that the means of studied populations of roughness parameters are equal for surfaces obtained at two voltages, i.e. 180 and 450 V. On the basis of the obtained roughness parameters, the probability "p" for all parameters was found. The lower the probability "p" from the level of significance (α), the hypothesis of equality of expected values must be rejected.

That way, all the proposed 2D roughness parameters such as the following: Ra ($p = 1.22 \cdot 10^{-4}$), Rz ($p = 5.21 \cdot 10^{-4}$), Rz^{ISO} ($p = 5.07 \cdot 10^{-4}$), Rq ($p = 1.17 \cdot 10^{-4}$), Rt ($p = 5.64 \cdot 10^{-4}$), RSm ($p = 2.89 \cdot 10^{-2}$), L ($p = 1.08 \cdot 10^{-4}$) and D ($p = 3.9 \cdot 10^{-2}$) are significantly different for two surfaces obtained at two voltages (180 and 450 V), and all of them can be used for these surface evaluations. However, the best roughness parameters for surface characterisation are Ra, Rz, Rz^{ISO}, Rq and L, what is confirmed by presented above the probability "p" and *box* and *whisker* plots in Fig. 24.

In Fig. 25, the XPS survey results of coating formed on Ti-Nb-Zr-Sn alloy after 3 min of PEO treatment at voltages 180 and of 450 V in electrolyte containing of H_3PO_4 within $Cu(NO_3)_2$ are presented. With that spectroscopic method, it is possible to detect the chemical elements from a depth of about 10 nm to find the oxidation stages of chemical elements constituting the PEO coating. Additionally, with that spectroscopic method, it is possible to separate the phosphorus and zirconium signals. On the basis of presented in Fig. 25 spectra, it was possible to conclude that in the first 10 nm of outer porous sub-layer, carbon-nitrogen-oxygen contaminations and the elements coming from the PEO coating, such as phosphorus and titanium, were recorded. In order to find the oxidation stages of chemical elements, high-resolution XPS measurements were performed and the results are presented in Figs. 26 and 27 and after quantitative analyses in Tables 3, 4,

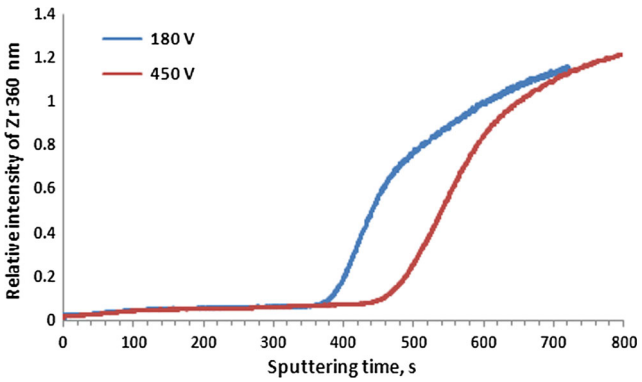

Fig. 20 GDOES results of zirconium signal (360 nm) of coating formed on Ti-Nb-Zr-Sn alloy after 3 min of PEO treatment at voltages of 180 and 450 V in electrolyte containing of H_3PO_4 within $Cu(NO_3)_2$

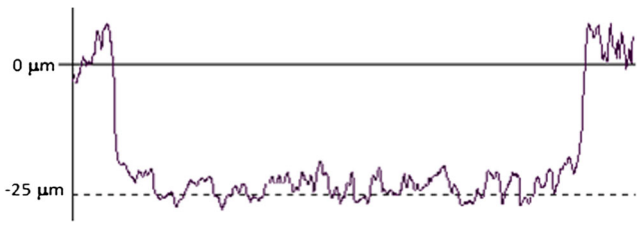

Fig. 22 The exemplary crater obtained after GDOES tests of coatings formed on Ti-Nb-Zr-Sn alloy after 3-min PEO treatment at voltage of 450 V in electrolyte containing of H_3PO_4 within $Cu(NO_3)_2$

Fig. 23 Two-dimensional profiles of coatings formed on Ti-Nb-Zr-Sn alloy after 3 min of PEO treatment at voltages of 180 and 450 V in electrolyte containing of H_3PO_4 within $Cu(NO_3)_2$

Table 1 Roughness parameters of PEO coating formed on Ti-Nb-Zr-Sn alloy treated at 180 V for 3 min in 3.2 mol/L of $Cu(NO_3)_2$ in H_3PO_4 electrolytes (the statistics made of 30 repetitions)

	180 V							
	Ra (μm)	Rz (μm)	Rz^{ISO} (μm)	Rq (μm)	Rt (μm)	RSm (μm)	L_0 (–)	D (–)
Mean	0.79	5.02	5.23	1.00	6.45	0.08	1.00	47.67
Variance	2E−04	0.15	0.08	1E−03	0.31	1E−05	3E−07	1.33
Sta. deviation	0.02	0.39	0.28	0.036	0.56	3E−03	6E−04	1.15
Median	0.79	5.24	5.38	1.01	6.67	0.083	1.003	47.00
Maximum	0.80	5.24	5.40	1.03	6.87	0.084	1.004	49.00
Minimum	0.77	4.57	4.91	0.96	5.82	0.079	1.003	47.00
Range	0.03	0.67	0.49	0.07	1.05	0.005	0.001	2.00

Table 2 Roughness parameters of PEO coating formed on Ti-Nb-Zr-Sn alloy treated at 450 V for 3 min in 3.2 mol/L of $Cu(NO_3)_2$ in H_3PO_4 electrolytes (the statistics made of 30 repetitions)

	450 V							
	Ra (μm)	Rz (μm)	Rz^{ISO} (μm)	Rq (μm)	Rt (μm)	RSm (μm)	L_0 (–)	D (–)
Mean	1.22	8.48	8.97	1.63	12.89	0.07	1.01	52.67
Variance	0.01	1.44	1.76	0.33	5.33	3E−05	3E−06	20.3
Sta. deviation	0.12	1.19	1.33	0.17	2.31	0.01	1E−03	4.51
Median	1.21	8.72	8.99	1.62	13.81	0.075	1.011	53.00
Maximum	1.35	9.54	10.29	1.8	14.59	0.08	1.011	57.00
Minimum	1.11	7.18	7.64	1.46	10.26	0.069	1.008	48.00
Range	0.24	2.36	2.65	0.34	4.33	0.011	0.003	9.00

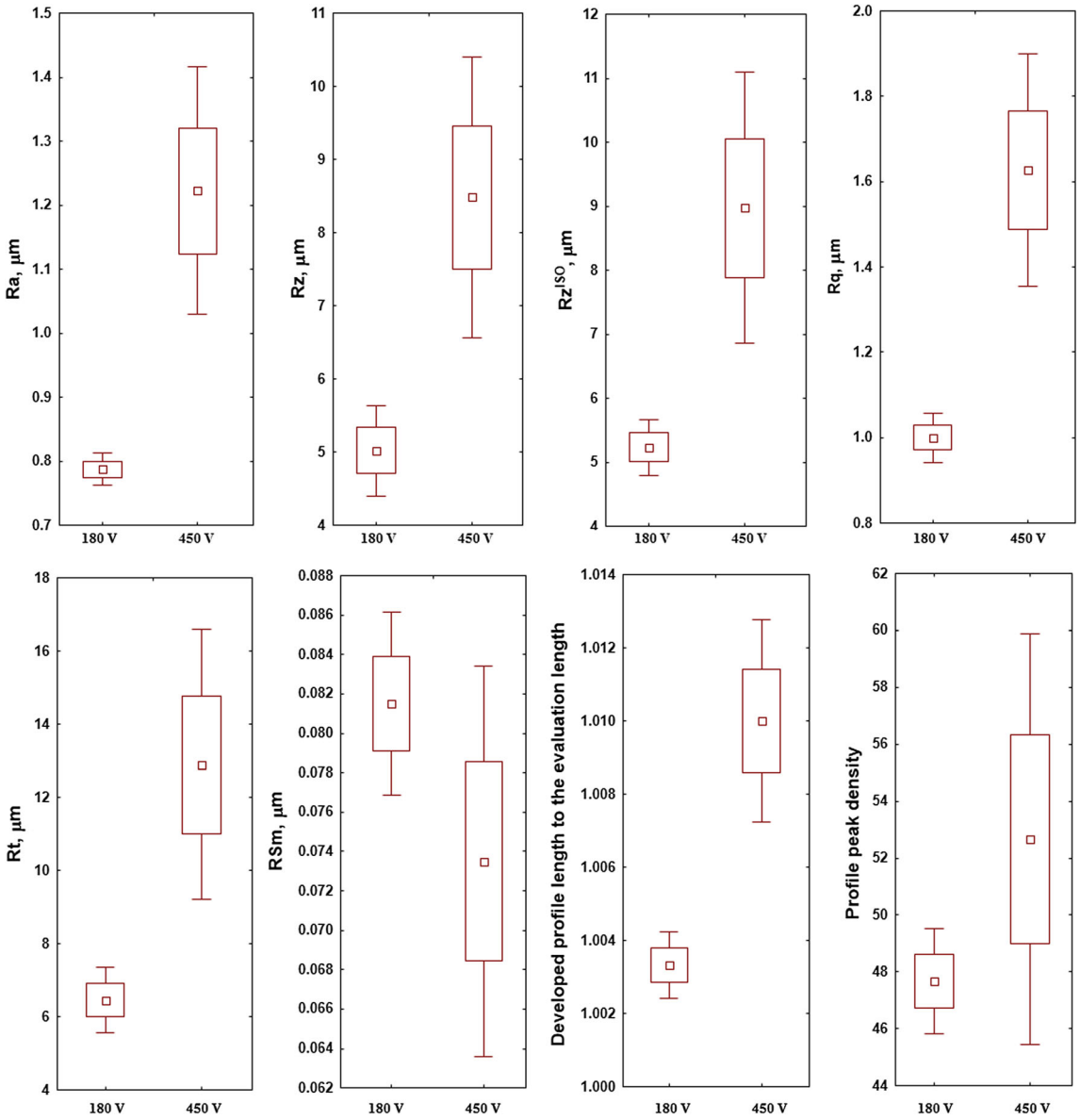

Fig. 24 *Box* and *whisker* plots of the roughness 2D parameters of the surface layer formed on Ti-Nb-Zr-Sn after PEO at voltages of 180 and 450 V in 3 min of PEO treatment in electrolyte containing 3.20 mol/L of $Cu(NO_3)_2$ in H_3PO_4 (the statistics made of three repetitions)

5 and 6. The chemical oxidation stages of the elements coming from the PEO coatings obtained both at 180 as 450 V are the same. The binding energies of oxygen O 1s (531.4 and 531.5 eV) and phosphorus P 2p (133.8 and 133.9 eV) clearly indicate the presence of phosphates of titanium and/or niobium and/or zirconium and/or copper in the PEO coatings. The binding energy of carbon (284.8 eV) and nitrogen (400.5 and 401 eV) can be identified as organic contaminations. The binding energies of main peaks for titanium Ti $2p_{3/2}$, niobium Nb $3d_{5/2}$ and zirconium Zr $3d_{5/2}$ are equal to 460–460.2, 207.9–208.1 and 183.6 eV, respectively, what suggests the presence of titanium Ti^{4+}, niobium Nb^{5+} and zirconium Zr^{4+} [43–46]. Tin present as a component of the alloy studied was not detected by XPS method in the outer 10 nm of PEO coatings.

On the basis of XPS results, which are presented in Tables 3 and 4, it may be concluded that in 10 nm of porous outer sub-layer, more phosphorus, oxygen, nitrogen, titanium and niobium after PEO treatment at 180 and 450 V were found. The amounts of copper and zirconium are very similar or the same, respectively. As it was recorded, the outer 10-nm sub-layer of the porous coating contains no tin inside.

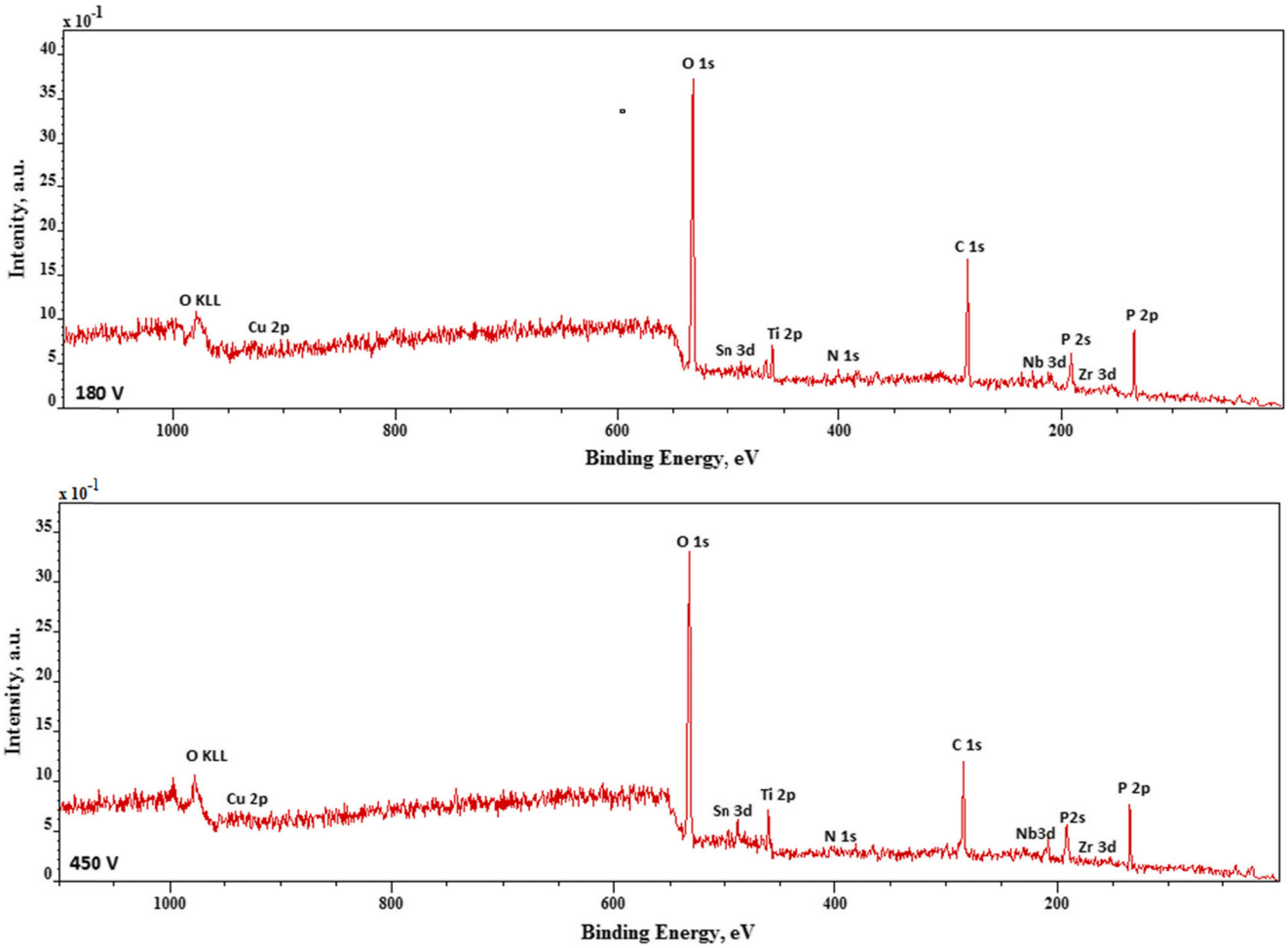

Fig. 25 XPS survey results of coating formed on Ti-Nb-Zr-Sn alloy after 3 min of PEO treatment at voltages 180 and of 450 V in electrolyte containing of H_3PO_4 within $Cu(NO_3)_2$

Because carbon as well as a part of the oxygen and nitrogen can be treated as organic contaminations, the authors propose finding the composition of obtained PEO coating only with matrix elements (titanium, niobium, zirconium, tin) as well as electrolyte elements (copper and phosphorus), what is shown in Tables 5 and 6. The highest differences are noted for phosphorus (3.9 at%) as well as for titanium (1.9 at%) and niobium (1 at%). In that outer and porous sub-layer, the same amount of zirconium and lack of tin were recorded.

The authors in the paper propose to use some ratios (1–2) to describe the obtained surfaces and allow to compare these XPS results with other ones from different researchers. The phosphorus to copper ratio (1) is very important, because these chemical elements do not come from the matrix, but only from the electrolyte used. In our results, the P/Cu ratio is higher for PEO treatment at 180 V (41.45) than that obtained after oxidation at 450 V (34.35). It can also be stated that in the coating obtained after PEO at 180 and 450 V, the phosphorus amounts are over 40 times or 30 times higher than the copper amounts, respectively:

$$\frac{\mathrm{P}}{\mathrm{Cu}} = \begin{cases} 41.45, & \text{for } U = 180\ \mathrm{V} \\ 34.35, & \text{for } U = 450\ \mathrm{V} \end{cases} \quad (1)$$

The second P/(Ti + Nb + Zr + Sn) ratio (2) describes the proportion of alloy elements in outer, phosphate, porous sub-layers. The result presented in this paper is that ratio is higher for PEO treatment at 180 V (5.49) than that obtained after oxidation at 450 V (4.39). It can be concluded that in the coating obtained after PEO at 180 and 450 V, the phosphorus amounts are over five times or four times higher than the sum of titanium, niobium, zirconium and tin amounts, respectively:

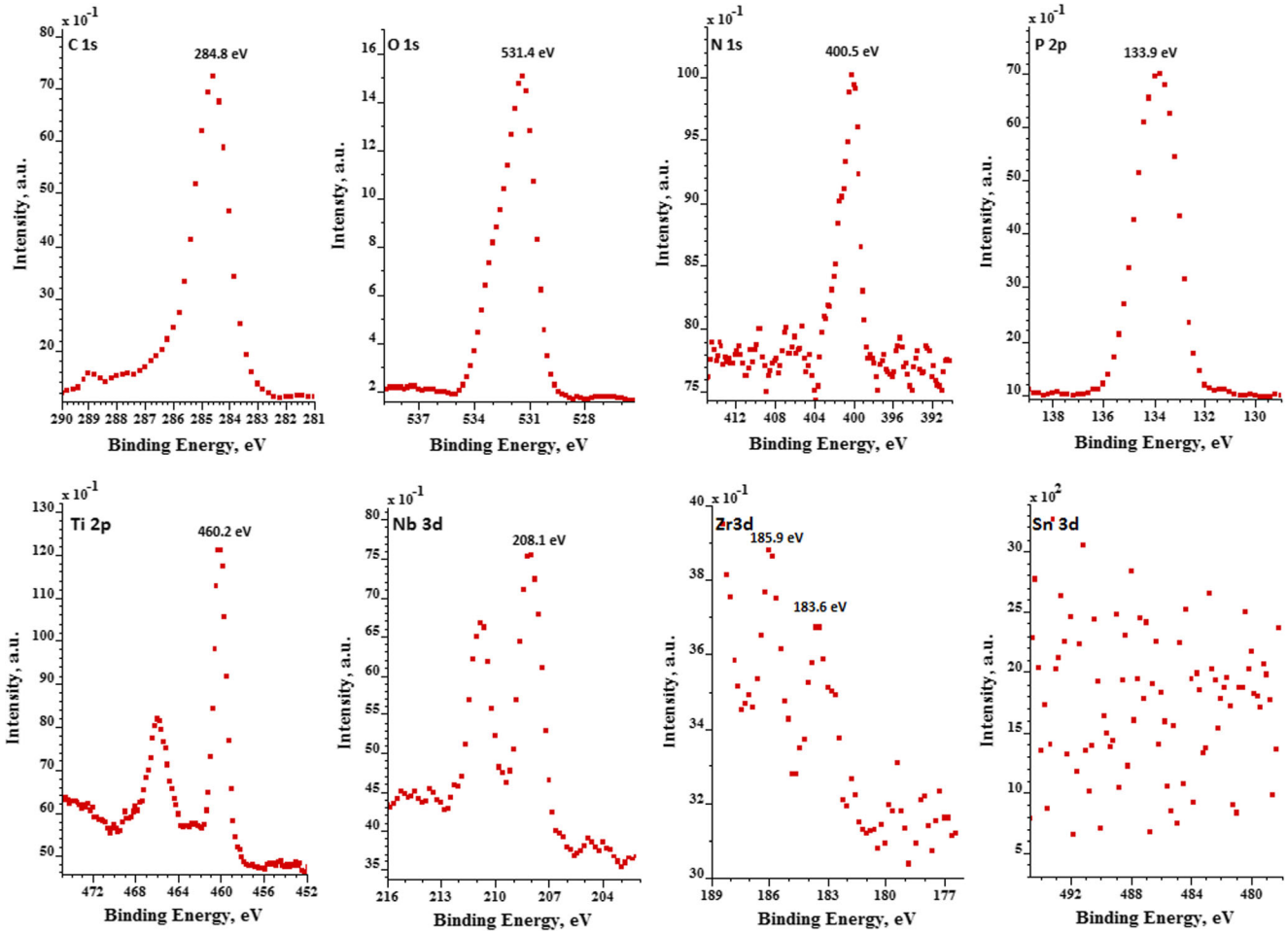

Fig. 26 High-resolution XPS spectra/results of coating formed on Ti-Nb-Zr-Sn alloy after 3 min of PEO treatment at voltage of 180 V in electrolyte containing of H_3PO_4 within $Cu(NO_3)_2$

$$\frac{\mathrm{P}}{\mathrm{Ti}+\mathrm{Nb}+\mathrm{Zr}+\mathrm{Sn}}=\begin{cases}5.49, & \text{for } U=180\ \mathrm{V}\\ 4.39, & \text{for } U=450\ \mathrm{V}\end{cases} \tag{2}$$

Based on (1) and (2) coefficients, it is possible to propose a model describing the composition of porous sub-layers, which have to be biocompatible and bactericidal, by the following mathematical relation:

$$\begin{cases}\begin{cases}\mathrm{Cu}\approx 0.024\cdot\mathrm{P}\\ \mathrm{Ti}+\mathrm{Nb}+\mathrm{Zr}+\mathrm{Sn}\approx 0.182\cdot P\end{cases} & \text{for } 180\ \mathrm{V}\\ \begin{cases}\mathrm{Cu}\approx 0.029\cdot\mathrm{P}\\ \mathrm{Ti}+\mathrm{Nb}+\mathrm{Zr}+\mathrm{Sn}\approx 0.228\end{cases} & \text{for } 450\ \mathrm{V}\end{cases} \tag{3}$$

By assuming that phosphorus amount is known, the amounts of copper as well as the sum of alloy elements (titanium, niobium, zirconium, tin) in PEO layers formed at 180 and 450 V may be determined by using the (3) mathematical relation.

In Fig. 28, the models of the coatings formed on Ti-Nb-Zr-Sn alloy after 3 min of PEO treatment at voltages of 180 and 450 V in electrolyte containing of H_3PO_4 within $Cu(NO_3)_2$ are presented. As it was mentioned, most likely, the coating can be divided into three sub-layers. The outer ones, porous, as obtained under both PEO treatments, i.e. at 180 and 450 V, containing compounds within Ti^{4+}, Nb^{5+}, Zr^{4+}, Cu^{+}, Cu^{2+}, PO_x and NO_x ions, have thicknesses equal to 3 μm. The second sub-layers, which are semi-porous, have thicknesses of 9 and 12 μm for the PEO voltages of 180 and 450 V, respectively. The third sub-layers, which are named transition layers, have the same thickness independent on the voltage applied, 180 or 450 V, equalling to 6 μm.

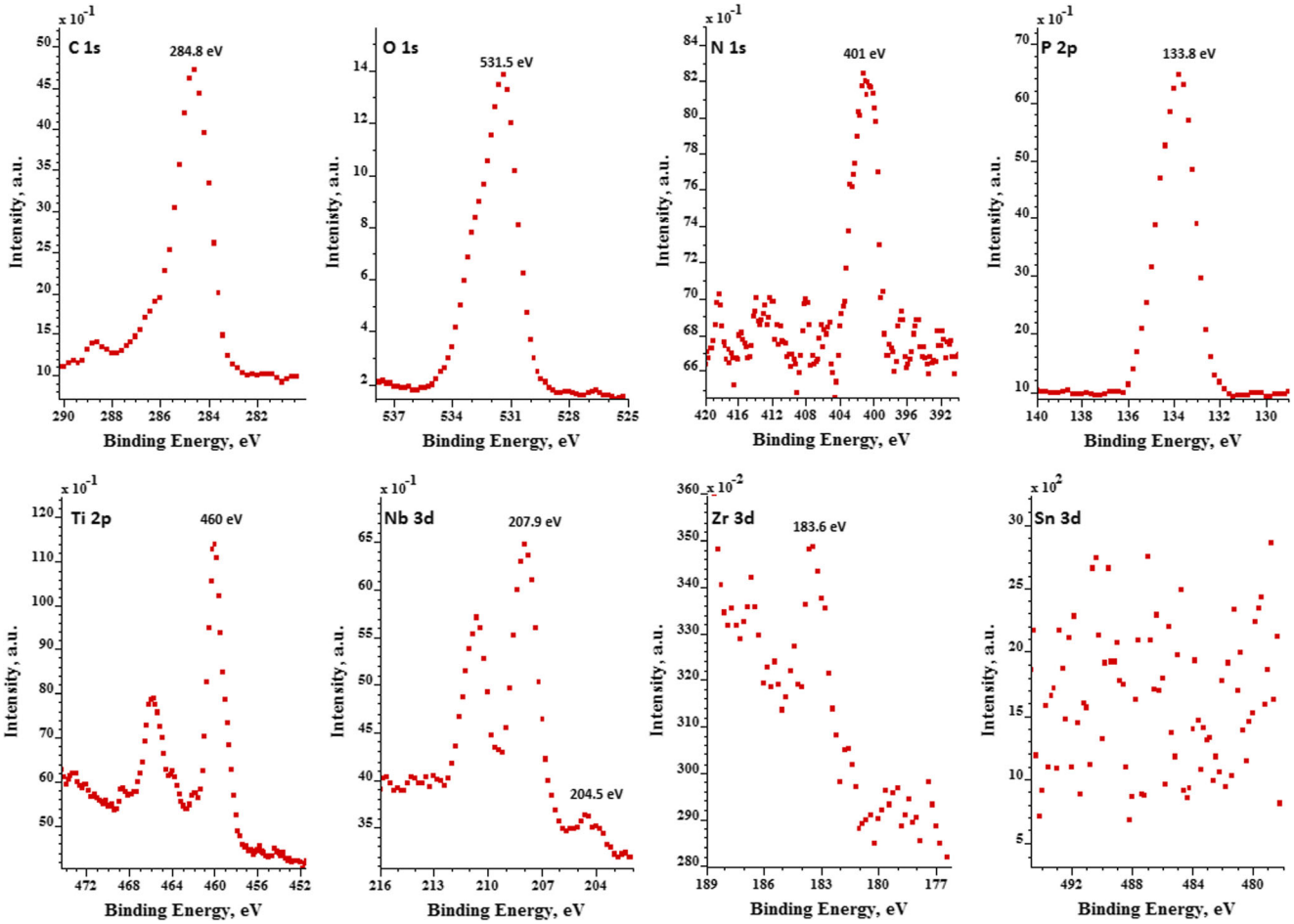

Fig. 27 High-resolution XPS spectra/results of coating formed on Ti-Nb-Zr-Sn alloy after 3 min of PEO treatment at voltage of 450 V in electrolyte containing of H_3PO_4 within $Cu(NO_3)_2$

Table 3 Total chemical composition of coating formed after PEO treatment at 180 V on Ti-Nb-Zr-Sn alloy with outer carbon- and bio-contaminations sub-layer, at% (based on XPS results)

Chemical composition of PEO layer formed on Ti-Nb-Zr-Sn alloy at voltage of 180 V, at% (information from depth up to 10 nm)								
Titanium	Niobium	Zirconium	Tin	Copper	Phosphorus	Oxygen	Nitrogen	Carbon
2.0	0.9	0.1	0	0.4	16.0	44.7	1.1	34.8

Table 4 Total chemical composition of coating formed after PEO treatment at 450 V on Ti-Nb-Zr-Sn alloy with outer carbon- and bio-contaminations sub-layer, at% (based on XPS results)

Chemical composition of PEO layer formed on Ti-Nb-Zr-Sn alloy at voltage of 450 V, at% (information from depth up to 10 nm)								
Titanium	Niobium	Zirconium	Tin	Copper	Phosphorus	Oxygen	Nitrogen	Carbon
2.5	1.1	0.1	0	0.5	16.4	48.6	2.0	28.8

Table 5 Atomic percent of titanium, niobium, zirconium, tin, copper and phosphorus in coating formed on Ti-Nb-Zr-Sn alloy after PEO treatment at 180 V, at% (based on XPS results)

Titanium	Niobium	Zirconium	Tin	Copper	Phosphorus
10.1	4.5	0.5	0	2.0	82.9

Table 6 Atomic percent of titanium, niobium, zirconium, tin, copper and phosphorus in coating formed on Ti-Nb-Zr-Sn alloy after PEO treatment at 450 V, at% (based on XPS results)

Titanium	Niobium	Zirconium	Tin	Copper	Phosphorus
12.0	5.5	0.5	0	2.3	79.0

Most likely the inner, transition sub-layers are formed at the beginning of PEO process; such created layers possess the same or very similar both their chemical composition and thickness. Most interesting is that inside these sub-layers, it is possible to detect a peak of copper, nitrogen, phosphorus and hydrogen, respectively. Such a finding may lead to the conclusion, with a high probability, that inside the PEO coating structure, there are also the molecules of phosphoric acid and copper nitrate. This phenomenon may be explained by formation of semi-porous sub-layers which can "close" some acid and/or salt molecules in the first seconds of that process (non-stable electrical condition, i.e. sharp peak of current during switch on of the voltage). During the next time of plasma oxidation, the semi-porous sub-layers are formed and their thickness can be correlated with the PEO process voltage: the higher is voltage, the quicker is coating formed. That way, after the PEO oxidation at 450 V, the thickness of that sub-layer is over 33 % higher than that obtained at 180 V. The outer porous sub-layer is formed at the end of the PEO treatment, most probably in the last seconds, during the switch off of the potential. That way also, the pores of these sub-layers have different shapes.

4 Conclusions

The following conclusions may be formulated after the PEO treatment of Ti-Nb-Zr-Sn alloy studied:

1. Porous coatings on titanium-niobium-zirconium-tin alloy surface, enriched in copper distributed in the whole volume, were obtained.
2. The PEO potential has an impact on the thickness of the coatings: the higher the potential used, the thicker coating was obtained.
3. The copper inside the coating appears as Cu^{+} and Cu^{2+} ions whereas titanium, niobium and zirconium occur as Ti^{4+}, Nb^{5+} and Zr^{4+}, respectively.
4. The coating is composed mostly of phosphorus and oxygen formed as phosphates of titanium and/or niobium and/or zirconium within copper ions.

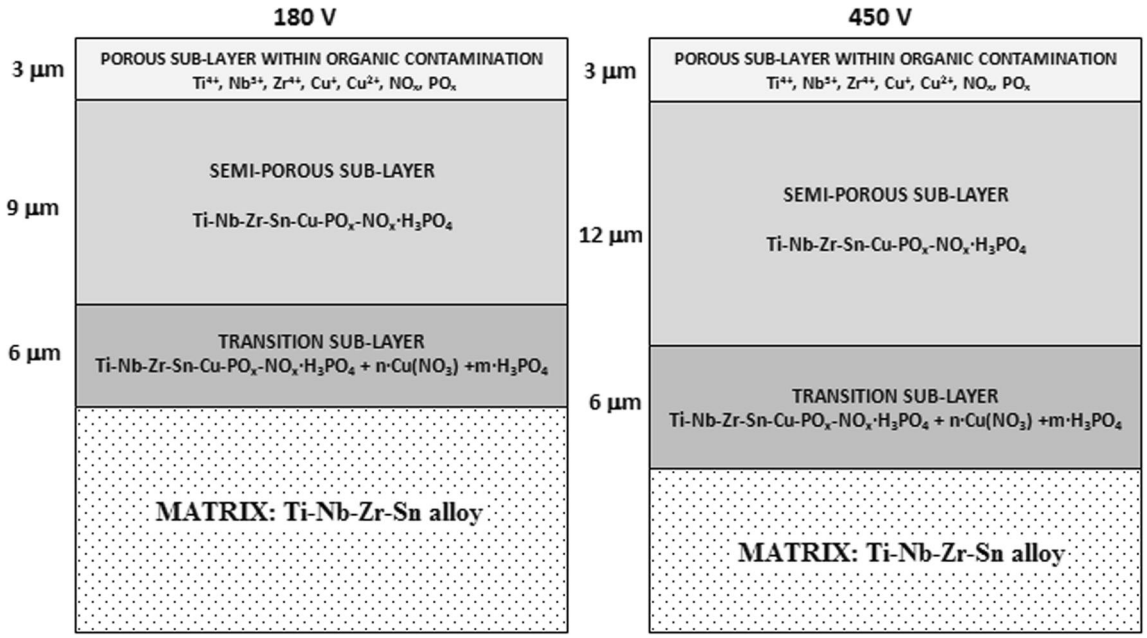

Fig. 28 Models of the coatings formed on Ti-Nb-Zr-Sn alloy after 3 min of PEO treatment at voltages of 180 and 450 V in electrolyte containing of H_3PO_4 within $Cu(NO_3)_2$

5. The roughness of PEO coating formed at 450 V is higher than that obtained at 180 V, and it is well correlated with bigger pores after the PEO treatment.
6. Three sub-layers, i.e. outer (porous), inner (semi-porous) and transition (adjacent to the matrix), may be separated in the PEO coating formed on Ti-Nb-Zr-Sn alloy.
7. The thickness of the outer porous sub-layer obtained after PEO oxidation at both 180 and 450 V equals to about 2.5 μm.
8. The semi-porous sub-layer is thicker after PEO processing at 450 V (12 μm) than that obtained at 180 V (9 μm).
9. The transition sub-layer thickness obtained at both PEO voltages, 180 and 450 V, is equal to about 6 μm.
10. It is most likely that the transition sub-layer, adjacent to the matrix, is formed at the very beginning of PEO treatment (switch on of the PEO potential); the second, semi-porous sub-layer, is formed during the stable voltage conditions of PEO treatment; the outer porous sub-layer is formed at the end of PEO treatment (switch off of the PEO potential).

Acknowledgments Prof. Dr Ing. Wienfried Malorny of Hochschule Wismar, Germany, is greatly acknowledged for making his labs accessible and valuable advice at SEM and EDS studies. Many thanks are directed to Professor Czesław Łukianowicz, DSc PhD, the Dean at the Faculty of Mechanical Engineering of KUT, for making available a computerized HOMMELTESTER T800 system of Hommelwerke GmbH. Acknowledgments are sent to Prof. Frédéric Prima, PSL Research University, ChimieParisTech—CNRS, Institut de Recherche de Chimie Paris, 75005, Paris, France, for the obtained TNZ samples used in this study.

References

1. Yerokhin AL, Nie X, Leyland A, Matthews A, Dowey SJ (1999) Plasma electrolysis for surface engineering. Surf Coat Technol 122(2–3):73–93. doi:10.1016/S0257-8972(99)00441-7
2. Simka W, Sadowski A, Warczak M, Iwaniak A, Dercz G, Michalska J, Maciej A (2011) Characterization of passive films formed on titanium during anodic oxidation. Electrochim Acta 56(27):8962–8968. doi:10.1016/j.electacta.2009.07.010
3. Jin FY, Tong HH, Shen LR, Wang K, Chu PK (2006) Microstructural and dielectric properties of porous TiO_2 films synthesized on titanium alloys by micro-arc discharge oxidization. Mater Chem Phys 100(1):31–33. doi:10.1016/j.matchemphys.2005.12.001
4. Simka W, Sowa M, Socha RP, Maciej A, Michalska J (2013) Anodic oxidation of zirconium in silicate solutions. Electrochim Acta 104:518–525. doi:10.1016/j.electacta.2012.10.130
5. Sowa M, Kazek-Kęsik A, Socha RP, Dercz G, Michalska J, Simka W (2013) Modification of tantalum surface via plasma electrolytic oxidation in silicate solutions. Electrochim Acta 144:627–636. doi:10.1016/j.electacta.2013.10.047
6. Simka W, Nawrat G, Chlode J, Maciej A, Winiarski A, Szade J, Radwański K, Gazdowicz J (2011) Electropolishing and anodic passivation of Ti6Al7Nb alloy. Przemysl Chemiczny 90(1):84–90
7. Yerokhin AL, Nie X, Leyland A, Matthews A, Dowey SJ (2000) Characterisation of oxide films produced by plasma electrolytic oxidation of a Ti–6Al–4V alloy. Surf Coat Technol 130(2–3):195–206. doi:10.1016/S0257-8972(00)00719-2
8. Wheeler JM, Collier CA, Paillard JM, Curran JA (2010) Evaluation of micromechanical behaviour of plasma electrolytic oxidation (PEO) coatings on Ti–6Al–4V. Surf Coat Technol 204(21–22):339–3409. doi:10.1016/j.surfcoat.2010.04.006
9. Yu S, Yu Z, Wang G, Han J, Ma X, Dargusch MS (2011) Preparation and osteoinduction of active micro-arc oxidation films on Ti-3Zr-2Sn-3Mo-25Nb alloy. Trans Nonferrous Metals Soc China 21:573–580. doi:10.1016/S1003-6326(11)60753-X
10. Rokosz K, Hryniewicz T, Raaen S (2015) Development of plasma electrolytic oxidation for improved Ti6Al4V biomaterial surface properties. Int J Adv Manuf Technol. doi:10.1007/s00170-015-8086-y
11. Hryniewicz T (1989) Physico-chemical and technological fundamentals of electropolishing steels (Fizykochemiczne i technologiczne podstawy procesu elektropolerowania stali). Monograph no. 26, ed. by Koszalin University of Technology Publishing: 161 pages
12. Hryniewicz T (2007) On the surface treatment of metallic biomaterials (Wstęp do obróbki powierzchniowej biomateriałów metalowych). Ed. by Koszalin University of Technology Publishing: 155 pages
13. Rokosz K (2012) Electrochemical polishing in the magnetic field (Polerowanie elektrochemiczne w polu magnetycznym). Ed. by Koszalin University of Technology Publishing: 211 pages
14. Hryniewicz T, Rokicki R, Rokosz K (2008) Co-Cr alloy corrosion behaviour after electropolishing and "magnetoelectropolishing" treatments. Surf Coat Technol 62(17–18):3073–3076. doi:10.1016/j.matlet.2008.01.130
15. Hryniewicz T, Rokosz K (2010) Analysis of XPS results of AISI 316L SS electropolished and magnetoelectropolished at varying conditions. Surf Coat Technol 204(16–17):2583–2592. doi:10.1016/j.surfcoat.2010.02.005
16. Hryniewicz T, Rokicki R, Rokosz K (2007) Magnetoelectropolishing for metal surface modification. Trans Inst Met Finish 85(6):325–332. doi:10.1179/174591907X246537
17. Hryniewicz T, Rokicki R, Rokosz K (2008) Corrosion and surface characterization of titanium biomaterial after magnetoelectropolishing. Surf Coat Technol 203(9):1508–1515. doi:10.1016/j.surfcoat.2008.11.028
18. Hryniewicz T, Rokosz K (2010) Polarization characteristics of magnetoelectropolishing stainless steels. Mater Chem Phys 122(1):169–174
19. Rokosz K, Hryniewicz T, Raaen S (2012) Characterization of passive film formed on AISI 316L stainless steel after magnetoelectropolishing in a broad range of polarization parameters. J Iron Steel Res 83(9):910–918
20. Hryniewicz T, Rokosz K (2010) Investigation of selected surface properties of AISI 316L SS after magnetoelectropolishing. Mater Chem Phys 123(1):47–55
21. Hryniewicz T, Rokosz K (2014) Corrosion resistance of magnetoelectropolished AISI 316L SS biomaterial. Anti-Corros Methods Mater 61(2):57–64
22. Hryniewicz T, Rokosz K, Valiček J, Rokicki R (2012) Effect of magnetoelectropolishing on nanohardness and Young's modulus

of titanium biomaterial. Mater Lett 83:69–72. doi:10.1016/j.matlet.2012.06.010
23. Hryniewicz T, Rokosz K, Rokicki R, Prima F (2015) Nanoindentation and XPS studies of titanium TNZ alloy after electrochemical polishing in a magnetic field. Materials 8:205–215. doi:10.3390/ma8010205
24. Rokosz K, Hryniewicz T, Simon F, Rzadkiewicz S (2015) Comparative XPS analysis of passive layers composition formed on AISI 304L SS after standard and high-current density electropolishing. Surf Interface Anal 47(1):87–92
25. Rokosz K, Lahtinen J, Hryniewicz T, Rzadkiewicz S (2015) XPS depth profiling analysis of passive surface layers formed on austenitic AISI 304L and AISI 316L SS after high-current-density electropolishing. Surf Coat Technol 276:516–520. doi:10.1016/j.surfcoat.2015.06.022
26. Rokicki R, Hryniewicz T, Pulletikurthi C, Rokosz K, Munroe N (2015) Towards a better corrosion resistance and biocompatibility improvement of Nitinol medical devices. J Mater Eng Perform 24:1634–1640. doi:10.1007/s11665-015-1429-x
27. Rokosz K, Hryniewicz T (2010) Pitting corrosion resistance of AISI 316L stainless steel in Ringer's solution after magnetoelectrochemical polishing. Corrosion 66(3):035004
28. Rokosz K, Hryniewicz T (2013) XPS measurements of LDX 2101 duplex steel surface after magnetoelectropolishing. Int J Mater Res 104(12):1223–1232. doi:10.3139/146.110984
29. Hryniewicz T, Konarski P, Rokosz K, Rokicki R (2011) SIMS analysis of hydrogen content in near surface layers of AISI 316L SS after electrolytic polishing under different conditions. Surf Coat Technol 205(17–18):4228–4236. doi:10.1016/j.surfcoat.2011.03.024
30. Hryniewicz T, Rokosz K, Zschommler Sandim HR (2012) SEM/EDX and XPS studies of niobium after electropolishing. Appl Surf Sci 263:357–361. doi:10.1016/j.apsusc.2012.09.060
31. Rokosz K, Hryniewicz T, Raaen S (2014) Cr/Fe ratio by XPS spectra of magnetoelectropolished AISI 316L SS fitted by Gaussian-Lorentzian shape lines. Tehnicki Vjesn-Tech Gaz 21(3):533–538
32. Rokosz K, Hryniewicz T, Raaen S (2015) SEM/EDX, XPS, corrosion and surface roughness characterization of AISI 316L SS after electrochemical treatment in concentrated HNO_3. Tehnicki Vjesn-Tech Gaz 22(1):125–131
33. Xiangyu Z, Xiaobo H, Ma Y, Lin N, Ailan F, Bin T (2012) Bactericidal behavior of Cu-containing stainless steel surfaces. Appl Surf Sci 258:10058–10063
34. Xiaohong Y, Xiangyug Z, Haibo W, Linhai T, Yong M, Bin T (2014) Microstructure and antibacterial properties of Cu-doped TiO_2 coating on titanium by micro-arc oxidation. Appl Surf Sci 292:944–947. doi:10.1016/j.apsusc.2013.12.083
35. Hempel F, Finke B, Zietz C, Bader R, Weltmann KD, Polak M (2014) Antimicrobial surface modification of titanium substrates by means of plasma immersion ion implantation and deposition of copper. Surf Coat Technol 256:52–58. doi:10.1016/j.surfcoat.2014.01.027
36. Zhua W, Zhang Z, Gu B, Sun J, Zhu L (2013) Biological activity and antibacterial property of nano-structured TiO_2 coating incorporated with Cu prepared by micro-arc oxidation. J Mater Sci Technol 29(3):237–244. doi:10.1016/j.jmst.2012.12
37. Parajulee S, Hayakawa M, Ikezawa S (2009) Adhesion strength of TiN stacked TiO_2 film correlated with contact angle, critical load, and XPS spectra. Plasma Fusion Res: Lett 4(055):055-1–055-4. doi:10.1585/pfr.4.055
38. Fernandez AM, Guzman AM, Vera E, Rodriguez Paez JE (2008) Efectos de fotodegradación propiciados por recubrimientos de TiO_2 y TiO_2 -SiO_2 obtenidos por Sol–gel. Bol Soc Esp Cerámica Vidrio V 47(5):259–266
39. Winship KA (1988) Toxicity of tin and its compounds. Adverse Drug React Acute Poisoning Rev 7(1):19–38
40. Rokosz K, Hryniewicz T, Dudek Ł, Matýsek D, Valíček J, Harničarova M (2016) SEM and EDS analysis of surface layers formed on titanium after plasma electrolytic oxidation in H_3PO_4 with the addition of $Cu(NO_3)_2$. J Nanosci Nanotechnol 16:1–4. doi:10.1166/jnn.2016.12558
41. Rokosz K, Hryniewicz T (2016) Plasma electrolytic oxidation as a modern method to form porous coatings enriched in phosphorus and copper on biomaterials. World Sci News 35:44–61
42. Casa Software Ltd (2009) CasaXPS: processing software for XPS, AES, SIMS and more. http://www.casaxps.com. (Accessed 26 June 2007)
43. Biesinger MC, Lau LWM, Gerson AR, Smart RSC (2010) Resolving surface chemical states in XPS analysis of first row transition metals, oxides and hydroxides: Sc, Ti, V, Cu and Zn. Appl Surf Sci 257:887–898. doi:10.1016/j.apsusc.2010.07.086
44. Rodenbücher Ch (2014) Resistive switching phenomena of extended defects in Nb-doped $SrTiO_3$ under influence of external gradients. Forschungszentrum Julich, Dissertation 38 RWTH Aachen University, ISSN 1866–1777, ISBN 978-3-89336-980-5, 79–80
45. Wagner C D, Naumkin A V, Kraut-Vass A, Allison J W, Powell C J, Rumble J R Jr (2003) NIST Standard Reference Database 20, Version 3.4 (2003) http://srdata.nist.gov/xps (Accessed 26 June 2007)
46. Boffa A B (1994) Transition metal oxides deposited on rhodium and platinum: surface chemistry and catalysis, center for advanced materials, Lawrence Berkeley Laboratory, University of California, PhD Thesis, LBL-35954, UC-401
47. Valiček J, Drzik M, Hryniewicz T, Harničarova M, Rokosz K, Kusnerova M, Barcova K, Brazina D (2012) Non-contact method for surface roughness measurement after machining. Meas Sci Rev 12(5):184–88. doi:10.2478/v10048-012-0028-3
48. Kusnerova M, Valicek J, Harničarova M, Hryniewicz T, Rokosz K, Palkova Z, Vaclavik V, Repka M, Bendova M (2013) A proposal for simplifying the method of evaluation of uncertainties in measurement results. Meas Sci Rev 13(1):1–6. doi:10.2478/msr-2013-0007
49. EN ISO 4287:(1999) Geometrical product specifications (GPS)—surface texture: profile method—terms, definitions and surface texture parameters. International Organization for Standarization
50. DIN 4768:(1990) Determination of values of surface roughness parameters Ra, Rz, Rmax using electrical contact (stylus) instruments; concepts and measuring conditions.